nant factor determining flux levels at those L values. By 2010 orbital debris absorption as a loss mechanism will be responsible for the shortest lifetimes below $L = 1.4$ and thus will be the most important factor determining the ambient fluxes of high-energy protons in the Van Allen belt.

The low-altitude regions of the magnetosphere are subject to solar cycle variations. Thus a test of the proposed hypothesis with appropriate radiation detector–bearing spacecraft will require the sampling of equatorial regions above about 700 km or at $1.2 < L < 1.7$.

REFERENCES AND NOTES

1. The data, provided by D. J. Kessler, have been corrected by a factor of 2 to compensate for a recently discovered error in the radar cross section measurements.
2. C. E. McIlwain, *J. Geophys. Res.* **66**, 3681 (1961).
3. R. S. White, *Rev. Geophys. Space Phys.* **11**, 595 (1973).
4. T. A. Farley *et al.*, *J. Geophys. Res.* **77**, 6087 (1972).
5. T. A. Farley and M. Walt, *ibid.* **76**, 8223 (1971).
6. D. J. Kessler and B. G. Cour-Palais, *ibid.* **83**, 2637 (1978).
7. G. D. Badhwar, personal communication.
8. International Association of Geomagnetism and Aeronomy Division I, Working Group 1, *Eos* **67**, 523 (1986).
9. A. J. Dragt, *J. Geophys. Res.* **76**, 2313 (1971).
10. M. Schulz and G. A. Paulikas, *ibid.* **77**, 744 (1972).
11. H. H. Heckman and P. J. Lindstrom, *ibid.*, p. 740.
12. I thank D. J. Kessler for providing the NASA/DOD Civil Needs Database data.

6 May 1988; accepted 28 September 1988

A Synchrotron X-ray Study of a Solid-Solid Phase Transition in a Two-Dimensional Crystal

SHARON GRAYER WOLF, MOSHE DEUTSCH, EHUD M. LANDAU,
MEIR LAHAV, LESLIE LEISEROWITZ, KRISTIAN KJAER, JENS ALS-NIELSEN

A measurement and interpretation on a molecular level of a phase transition in an ordered Langmuir monolayer is reported. The diagram of surface pressure (π) versus molecular area of a monolayer of chiral (*S*)-[CF_3–$(CF_2)_9$–$(CH_2)_2$–OCO–CH_2–$CH(NH_3^+)CO_2^-$] over water shows a change in slope at about $\pi_s = 25$ millinewtons per meter. Grazing-incidence x-ray diffraction and specular reflectivity measurements indicate a solid-solid phase transition at π_s. The diffraction pattern at low pressures reveals two diffraction peaks of equal intensities, with lattice spacings *d* of 5.11 and 5.00 angstroms; these coalesce for $\pi \geq \pi_s$. Structural models that fit the diffraction data show that at $\pi > \pi_s$ the molecules pack in a two-dimensional crystal with the molecules aligned vertically. At $\pi < \pi_s$ there is a molecular tilt of 16° ± 7°. Independent x-ray reflectivity data yield a tilt of 26° ± 7°. Concomitant with the tilt, the diffraction data indicate a transition from a hexagonal to a distorted-hexagonal lattice. The hexagonal arrangement is favored because the –$(CF_2)_9CF_3$ moiety adopts a helical conformation. Compression to 70 millinewtons per meter yields a unit cell with increased crystallinity and a coherence length exceeding 1000 angstroms.

A LARGE VARIETY OF LANGMUIR monolayers at the air-water interface show sharp discontinuities in their surface pressure–molecular area (π-*A*) diagrams that are indicative of phase transitions (*1*). However, structural studies at the molecular level have until now been hampered by experimental difficulties. Grazing-incidence x-ray diffraction and specular reflectivity measurements (*2–10*) have recently become important tools for the structural investigation of Langmuir monolayers. We have performed such measurements on monolayers of compound **1**

$$CF_3–(CF_2)_9–(CH_2)_2–OCO–CH_2–CH(NH_3^+)CO_2^-$$

at the air-water interface, using the liquid surface diffractometer at the synchrotron x-ray beamline D4, Hasylab, Deutches Elektronen-Synchrotron (DESY), Hamburg.

This compound was chosen for study for the following reasons. The π-*A* diagram of **1** (Fig. 1) shows a change in slope at a surface pressure of 20 to 30 mN/m which we designate as π_s, corresponding to $A = 30$ to 35 Å^2. Compound **1** is one of a series of α-amino acid surfactants that were designed for the study of oriented crystallization of the α-form of glycine at the monolayer-water interface (*11*). The induced crystallization of α-glycine at the interface under the monolayer in various states of compression indicated a mismatch between the packing arrangement of the glycyl head groups of **1** and that of α-glycine. Thus we studied the monolayer by x-ray methods to elucidate, at a molecular level, its structure on both sides of the phase transition. In terms of x-ray scattering, **1** has several advantages for structural determination. The fluorocarbon chain has a much higher x-ray scattering power than the corresponding hydrocarbon chain and is more rigid. Further, the glycyl head groups should, by virtue of intermolecular hydrogen bonding, "fix" the molecular packing in the monolayer, preventing rotational disorder.

Monolayers of **1** were spread from solutions in chloroform:trifluoroacetic acid (96:4) onto a water surface in a temperature-controlled Langmuir trough placed on the diffractometer and maintained at 20°C. Details of the experimental conditions are given elsewhere (*3, 9*). At high π one peak appeared (Fig. 2); as pressure was decreased, the peak shifted position, widening and becoming less intense, until at about 25 to 30 mN/m it split into two peaks. The phase transition is clearly indicated by the *d* spacings, which along with the integrated intensities and the peak half-widths [inversely related to the coherence length *L* by the Scherrer formula (*12*)] are displayed as a function of surface pressure in Fig. 3. The increase in half-width at lower π is accompanied by a 60% decrease in integrated intensity. Rotation of the sample around an axis normal to the water surface showed that the monolayer is a two-dimensional powder. No other diffraction peaks were detected in

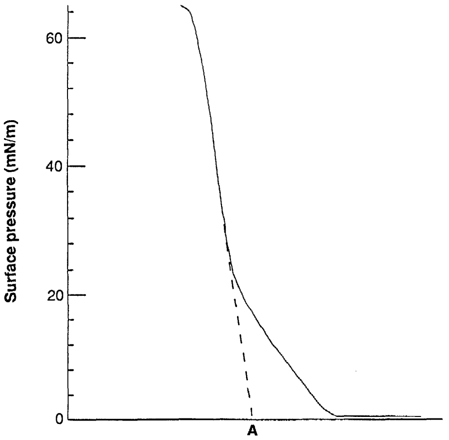

Fig. 1. Diagram of surface pressure versus surface area (π-*A*) of compound **1** at 20°C. Solubility problems lead to unreliability in the concentration of solutions of **1**, and therefore of the measurement of molecular area in the isotherm. Thus no values are given. The limiting area per molecule (*A*) was assigned from the x-ray diffraction data (28.5 Å^2 per molecule).

S. Grayer Wolf, E. M. Landau, M. Lahav, L. Leiserowitz, Structural Chemistry Department, Weizmann Institute of Science, Rehovot 76100, Israel.
M. Deutsch, Physics Department, Bar-Ilan University, Ramat Gan 52100, Israel.
K. Kjaer and J. Als-Nielsen, Physics Department, Risø National Laboratory, DK4000 Roskilde, Denmark.

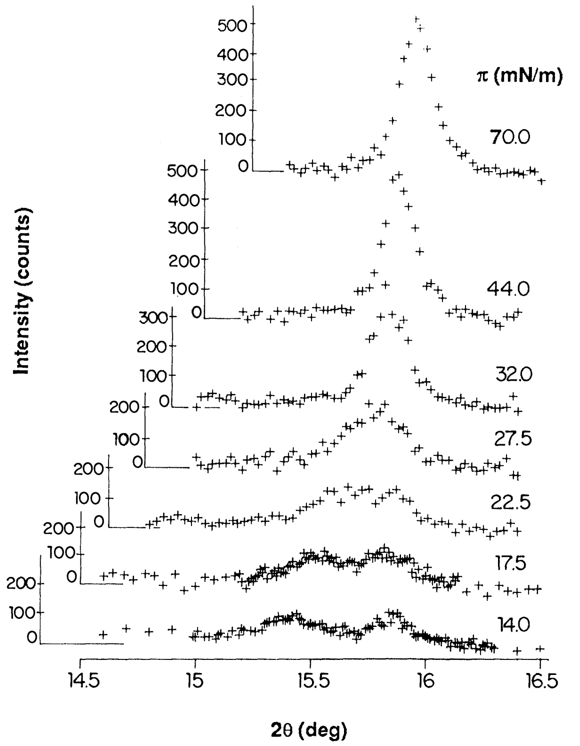

Fig. 2. Grazing-angle diffraction data measured for Langmuir monolayers of compound **1** at the surface pressures indicated. The wavelength used was 0.138 nm. A background of 150 counts was subtracted from each data set. Details of the experimental setup are described elsewhere (*3*).

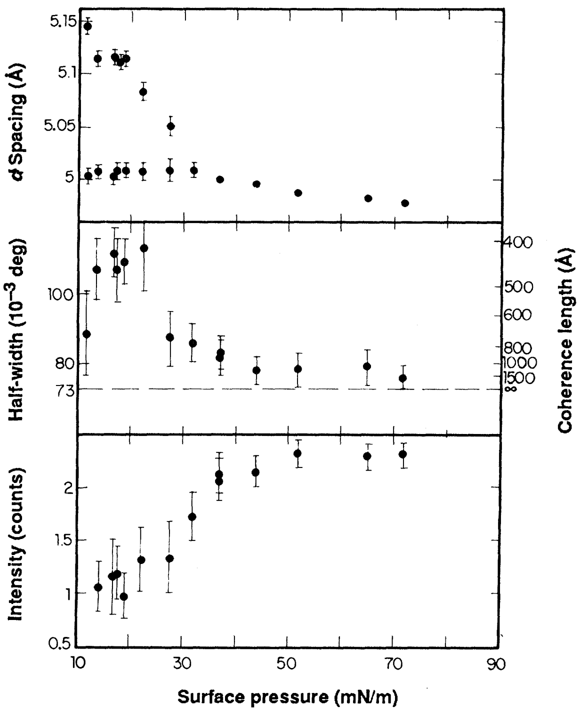

Fig. 3. The measured *d* spacing, peak half-width at half maximum (HWHM), and integrated intensity, as a function of surface pressure. In the low-π phase, equal widths were assumed for both peaks, an assumption justified by a separate analysis that allowed for unequal widths. The broken line in the middle panel indicates the resolution limit, and the right-hand scale gives the coherence length *L* [see (*11*)]. The error bars indicate ± 1 SD in the values as obtained from nonlinear least squares fits of the peaks of Fig. 2 to Lorentzian line shapes, which were found to represent the data well.

the range of $10° < 2\theta < 40°$, where θ is the diffraction angle.

Because about two-thirds of the length of **1** consists of the perfluorinated chain (the molecular cross-sectional area of which is likely to be larger than that of the aspartate residue), it seemed reasonable that this segment would be dominant in the crystal packing. Thus we took as a starting point the known structure of the perfluorinated polymer polytetrafluoroethylene (PTFE). Stretched films of PTFE, as examined by x-ray diffraction (*13, 14*), show the polymer chains to be arranged in a hexagonal lattice with $a = b = 5.65$ Å, having a molecular cross-sectional area of 27.6 Å^2. The chains adopt a helical conformation with a twist of 13° to 15° per C–C bond, depending on temperature. Calculations on *n*-perfluoroalkane molecules show that such a helical twist lowers the intramolecular energy by about 0.8 kJ/mol per bond and thus confirm the helical chain as the preferred conformation (*15*). This helicity appears to be an inherent characteristic of the molecule, and not a property due to crystal packing forces (*15, 16*).

It has been postulated that the helicity arises from reduction of intramolecular steric hindrance between fluorine atoms in the 1,3 positions (*13*) and from bond dipole-dipole repulsion (*15*). Therefore, a helical structure incorporating a 15° twist per C–C bond is the favored one for the perfluorinated section of the monolayer molecules. Such a conformation would imply a hexagonal cell because of the approximately cylindrical outer surface of the fluorocarbon segment (see Fig. 4). Indeed, the grazing-angle x-ray diffraction experiments at high surface pressures revealed only one diffraction peak with a *d* spacing of 4.97 Å. This indicates a hexagonal lattice with coinciding reflections (1,0), (0,1), and (1,−1), with unit cell $a = b = 5.75$ Å and a molecular area $ab \sin\gamma = 28.5$ Å^2, which is large enough to accommodate the helical perfluorinated segment. This cell for the high-π phase is also in keeping with the x-ray powder diffraction pattern of three-dimensional crystalline **1**, which contains a very strong reflection at $d = 4.91$ Å. Assuming the chain axis to be normal to the water surface yields a molecular height of 21.7 Å. This molecular height directly correlates to the layer spacing of 21.7 Å derived from the x-ray powder pattern of crystalline **1**, although the comparison is not straightforward because we cannot determine at present the degree of interleaving between terminal CF_3 groups of neighboring layers in the crystal. As discussed below, modeling of the reflectivity data of the high-π phase reveals a molecular height of 21.3 Å (see Table 1), also in good agreement with the above value. The molecular area (28.9 Å^2) derived from the reflectivity data also is in good agreement with the area of the unit cell (28.5 Å^2) as derived from the diffraction data.

Upon decompression, two x-ray diffraction peaks were observed at low surface pressures ($\pi = 10$ to 20 mN/m) with *d* spacings of 5.11 and 5.00 Å, and an intensity ratio of 1:1 (± 0.5). We propose a single-phase model in which the hexagonal lattice observed at high pressure is distorted by a tilt of the molecules on the reduction of pressure.

Distortions along nonsymmetry directions are ruled out because they would result in three low-order powder peaks. Figure 4 shows schematically the high-π hexagonal lattice (model H) and the two possibilities (models I and II) for distortion along symmetry directions. In these three cases, $d(1,0)$ and $d(0,1)$ are always equal. The molecules may tilt toward their nearest neighbors either in the $a + b$ direction (model I), leaving the $d(1,-1)$ spacing unchanged and increasing $d(0,1) = d(1,0)$, or they may tilt in the $a - b$ direction (model II), increasing both $d(1,-1)$ and $d(0,1) = d(1,0)$ but unequally. Either lattice will yield only two diffraction peaks, with a measured integrated intensity ratio of

$$r = r_0/r_1 \qquad (1)$$

where

$$r_0 = \int d\ell[|F(1,0,\ell)|^2 + |F(-1,0,\ell)|^2 + |F(0,1,\ell)|^2 + |F(0,-1,\ell)|^2]$$

and

$$r_1 = \int d\ell\,[|F(1,-1,\ell)|^2 + |F(-1,1,\ell)|^2]$$

In Eq. 1, $|F|^2$ denotes the squared structure factor corrected by the beam cross-sectional area factor $1/\sin 2\theta$ and the Lorentz-polarization factor $\cos^2 2\theta/\sin 2\theta$. The integration over the vertical component (ℓ) of the scattering vector accounts for the vertical resolution (3.8°) of the detector. At a molecular tilt of 0°, r should be ≈ 2.

The ratio r was calculated for the two models as a function of molecular tilt, where the following molecular model was assumed. The ester group, ($C_2H_4CO_2CH_2$), in the lower segment of the chain was assumed to conform to an all-*trans* conformation. The conformation of the glycyl head group, [$CH(NH_3^+)CO_2^-$], relative to the ester moiety was optimized by energy minimization with atom-atom potential energy calculations that included electrostatic terms (*17*). The in-plane orientation of the molecule in relation to the a and b axes is shown in Fig. 4. For model II, the calculations show that the ratio rapidly increases from $r = 2$ at 0° tilt to $r > 10$ at 20° tilt. This does not correlate with the observed intensity ratio of 1:1 (± 0.5). In contrast, for model I the ratio r decreases as a function of tilt. A tilt of 16° ± 7° (mean ± SE) corresponds to the observed ratio of $r = 1:1$ (± 0.5). The uncertainty arises from the ambiguity in the orientation of the molecule about the vertical axis, which does not allow us to distinguish between tilting in the ($a + b$) direction and tilting in the $-(a + b)$ direction. Model I is therefore the favored structure, leading to a unit cell of $a = b = 5.815$ Å, $\gamma = 118.5°$, and a molecular area $ab \sin\gamma = 29.7$ Å^2 for the low-π phase. The intermolecular F ··· F contacts in this model are acceptable, averaging 2.8 Å with a minimum of 2.6 Å. The relative change in $|\mathbf{a} + \mathbf{b}|$, $(1 + \epsilon) = 5.98/5.74 = 1.042$ (Fig. 4), corresponds through $\cos(t) = 1/(1 + \epsilon)$ to a tilt angle $t = 16°$, on the assumption that the original contacts between chains in model H are preserved as π is lowered. This is in excellent agreement with the value of 16° ± 7° derived from the calculated intensity ratio.

Direct evidence for a molecular tilt comes from an analysis of the specular reflectivity data. The measured intensity is related to the variation in the electron density distribution normal to the surface plane (*2*). The reflectivity curves show a significant change as a function of π (Fig. 5a and Table 1). At each value of π a three-box model describing the vertical electron density distribution of the monolayer was refined for the best fit to the reflectivity data. The three boxes correspond to the glycyl, ester, and fluorocarbon groups with 37, 46, and 249 electrons, respectively. The electron density is smeared by a Gaussian term of width σ (analogous to the Debye-Waller factor in x-ray crystallography) (Fig. 5b and Table 1). Five parameters were refined for each model: σ, the molecular area, and the length of each of the three boxes. Further details of the method are described elsewhere (*2*). Table 1 shows that the projected length ℓ(M) of the molecule increases with increased π. The estimated tilt of the molecule at low surface pressure is 26° ± 7°, as derived from the average calculated molecular heights ($<\ell_m>$) of the low-π and high-π phases.

The data in Table 1 indicate, however, that the molecules do not tilt rigidly. The decompression induces conformational changes mainly in the glycyl and ester groups, as indicated by the large decrease in length in the former and the lack of it in the latter. A comparison of the electron density profiles derived from the box model and the molecular model described above shows that the ester group is compressed by about 30% from the all-*trans* conformation assumed in the molecular model. It is possible to envisage the ester group folding so as to optimize intra- and intermolecular contacts.

Returning now to the in-plane diffraction measurements, we note that in the low-π phase the estimated L value of the two-

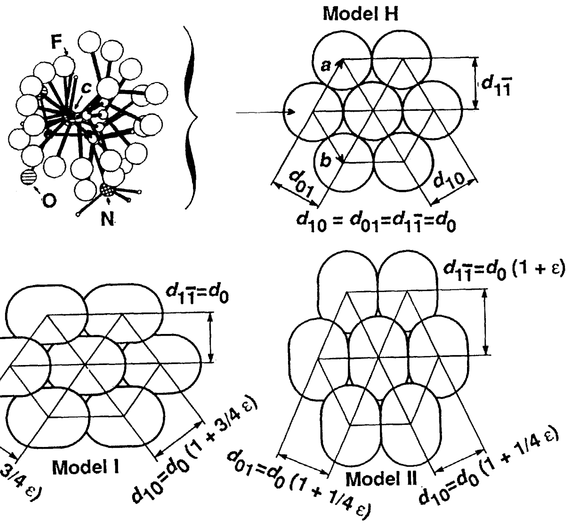

Fig. 4. Top view of the model molecule (top left) and schematic top views of the high-π structure (model H) and the two models (models I and II) for the low-π structure (see text).

Table 1. Refined electron density profiles based on measured reflectivity data, where π is the maintained surface pressure; ℓ(H), ℓ(E), ℓ(T), and ℓ(M) are the head, ester, tail, and total model molecular lengths, respectively; and ρ is the number of electrons per ℓ per A_{refl}, where A_{refl} is the molecular area from reflectivity data. The number of electrons per volume of water is $w = 0.334$ electron/Å^3; A_{dif} is the molecular area calculated from the model unit cells of the low- and high-π phases. For runs a through d, $A_{\text{dif}} = 26.6$ Å^2; runs for f through i, $A_{\text{dif}} = 29.7$ Å^2. The transition point is at e; σ is the Gaussian root-mean-square roughening. Typical uncertainities in these values are 0.1 Å, 0.05, 1 Å^2, and 0.3 Å for ℓ, ρ, area, and σ, respectively. The least-squares fits achieved equally weighted χ^2 values of order 0.02 or better. The tilt (t) is calculated from: $\cos(t) = <\ell(M)>_{\pi<\pi s}/<\ell(M)>_{\pi>\pi s} = 18.79/20.99$. Thus $t = 26.5°$ for the low-π phase.

Run	π (mN/m)	ℓ(H) (Å)	ℓ(E) (Å)	ℓ(T) (Å)	ℓ(M) (Å)	ρ_H/w	ρ_E/w	ρ_T/w	A_{refl} (Å)	$A_{\text{dif}}/A_{\text{refl}}$	σ (Å)
a	66	2.4	4.3	14.6	21.3	1.6	1.1	1.8	29	0.99	
2.7											
b	44	2.3	4.3	14.5	21.2	1.6	1.1	1.8	29	0.99	2.6
c	35	2.2	4.4	14.0	20.6	1.7	1.1	1.8	29	0.99	2.8
d	35	2.3	4.2	14.5	20.9	1.6	1.1	1.7	30	0.95	2.6
e	22	1.4	4.3	12.8	18.5	2.3	1.0	1.8	33		3.0
f	18	1.8	3.9	13.5	19.2	1.8	1.0	1.6	34	0.87	2.9
g	12	1.7	3.8	12.8	18.3	1.8	1.0	1.6	36	0.82	2.4
h	12	1.9	3.9	13.5	19.3	1.7	1.1	1.7	34	0.88	2.2
i	10	1.6	4.1	12.6	18.3	2.0	1.0	1.8	34	0.88	2.8

dimensional crystalline structure is approximately 400 Å, according to the measured reflection widths (*12*). In the high-π phase, the peak half-width approaches the resolution limit of 0.073° (marked in Fig. 3 by the broken line) as L exceeds 1000 Å. The increase in the integrated intensities of the diffraction peaks in the high-π phase, by about 2.5-fold, suggests a much higher degree of order (that is, a lower effective Debye-Waller factor) above the transition point. This conclusion holds even when we take account of the 10% increase in monolayer coverage and a 50% increase in the sum of squared structure factors that result from the straightening of the molecules with surface pressure. Thus we interpret the transition upon decompression as a combination of molecular tilting and the release of molecules from a more rigid conformation with higher molecular ordering.

The discrepancy between the area per molecule as determined by the diffraction and the reflectivity data ($A_{\mathrm{dif}}/A_{\mathrm{refl}}$ in Table 1) indicates <86% monolayer coverage of the water surface at low π. It is unclear at this stage whether the uncovered area is composed of point defects or of larger uncovered "patches."

In stretched polymers of PTFE at 20°C a transformation occurs from a structure in a pseudo-hexagonal cell in which all molecules have the same orientation to a truly hexagonal structure in which the molecular orientation about the chain axis is random (*13*). An analogous type of disorder in the high-π form of **1** is prevented by the zwitterionic glycyl moieties that are interlinked by two NH ··· O (carboxylate) hydrogen bonds. These bond vectors are likely to be 120° apart and coincident with the vector directions b and $a + b$ (see Fig. 4). Although the optimal molecular area for hydrogen bonding of the glycyl moiety (25 Å^2) is smaller than that found for monolayer **1** (28.5 Å^2), reasonable hydrogen bonds can still be formed. The monolayer may contain molecules with both left- and right-handed twists of the fluorocarbon chain. However, analysis of the reflectivity data indicated compression of the ester group, requiring a twist of the backbone chain. Then the chirality about the asymmetric carbon atom in the glycyl moiety should fix the sense of the ester group twist, which in turn should fix the chiral sense of the fluorocarbon chain.

The packing arrangement of monolayer **1** provides an explanation of the crystallization behavior of α-glycine grown underneath the monolayer (*11*). It was found that α-amino acid monolayers such as palmitoyl-lysine of, say, *S*-configuration, induced perfect epitaxial nucleation of α-glycine by virtue of the excellent match between their layer structures, whereby only (0,−1,0) crystal faces were attached. On the other hand, monolayers of **1** caused incompletely oriented attachment of α-glycine, with the ratio of attachment of the faces (0,−1,0) and (0,1,0) about 65/35. This can be understood in terms of the mismatch between the layer structures of **1** and α-glycine. First, the cell axes of the monolayer ($a = b = 5.74$ Å, $\gamma = 120°$) do not closely fit those of α-glycine ($a = 5.10$ Å, $c = 5.46$ Å, $\beta = 111.7°$). Moreover, the orientation of the glycyl head groups of **1** relative to the water surface should be distinctly different from that of α-glycine in its layer structure, because of the vertical orientation of **1** in the monolayer.

In conclusion, synchrotron x-ray scattering experiments with vertical and horizontal scattering vectors show a phase transition upon decompression in a surfactant monolayer from a structure with vertical molecular axes and long-range positional coherence ($L > 1000$ Å) to a structure with tilted molecules and medium coherence length ($L \sim 400$ Å). A comparison of the data with model calculations made it possible to assign the main features of the structures of the two phases. Phase transitions have also recently been observed in surfactant monolayers of fatty acids (*18, 19*).

Finally, we have briefly alluded to the match between the monolayer structure of **1** and its three-dimensional counterpart. A similar match was found for palmitoyl-(*S*)-lysine (*9*). It remains to be seen to what degree the similarity in packing arrangements between amphiphilic monolayers and the corresponding three-dimensional crystals is a universal property.

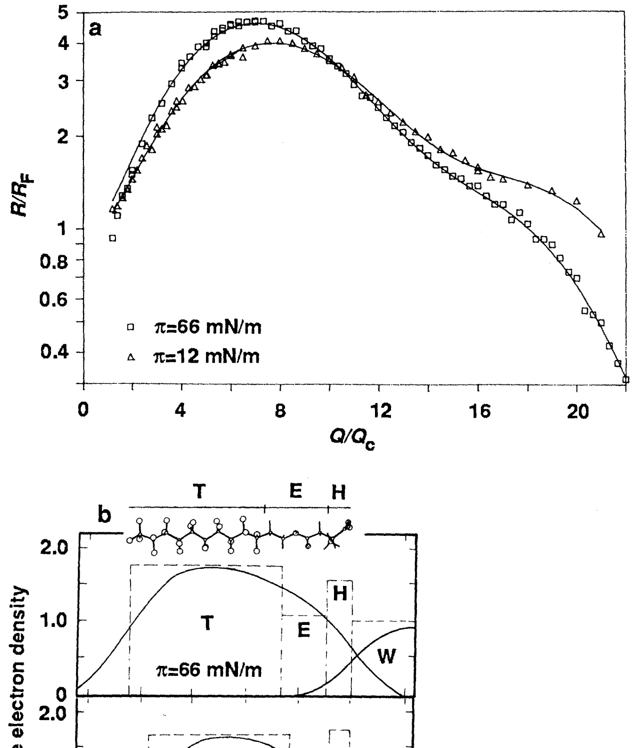

Fig. 5. (**a**) Reflectivity data from the low-π phase at 12 mN/m (△) and the high-π phase at 66 mN/m (□), with the fitted model reflectivity (—) for each, derived from parameters in Table 1. R, measured reflectivity; R_F, Fresnel reflectivity of an ideally smooth and abrupt surface (*2*); Q, vertical wavevector transfer; Q_c, wavevector transfer corresponding to the critical angle for total external reflection. (**b**) Refined relative electron density profile $\rho(z)$ versus z (where z is the vertical direction) [with $\rho(\text{water}) = 1$], which was fitted to the reflectivity data for $\pi = 66$ mN/m and 12 mN/m (see Table 1), with the fluorocarbon tail (T), the ester group (E), and the glycyl head group (H) indicated. The contribution of the water subphase (W) to $\rho(z)$ is also shown. At the top is shown the side view of the molecule with no tilt, corresponding to the high-π phase; the oxygen atoms are darkened.

REFERENCES AND NOTES

1. G. L. Gaines, Jr., *Insoluble Monolayers at Liquid-Gas Interfaces* (Wiley, New York, 1966).
2. J. Als-Nielsen, in *Topics in Current Physics*, W. Schommers and P. von Blanckenhagen, Eds., vol. 2, *Structure and Dynamics of Surfaces* (Springer-Verlag, Berlin, 1986), chap. 5, pp. 181–222.
3. S. Grayer Wolf *et al.*, *Nature* **328**, 63 (1987).
4. K. Kjaer *et al.*, *Phys. Rev. Lett.* **58**, 2224 (1987).
5. P. Dutta *et al.*, *ibid.*, p. 2228.
6. C. A. Helm, H. Möhwald, K. Kjaer, J. Als-Nielsen, *Europhys. Lett.* **4**, 697 (1987).
7. ———, *Biophys. J.* **52**, 381 (1987).
8. R. M. Richardson and S. J. Roser, *Liq. Cryst.* **2**, 797 (1987).
9. S. Grayer Wolf *et al.*, *Thin Solid Films* **159**, 29 (1988).
10. K. Kjaer, J. Als-Nielsen, C. A. Helm, P. Tipmann-Krayer, H. Möhwald, *ibid.*, p. 17.
11. E. M. Landau, M. Levanon, L. Leiserowitz, M. Lahav, J. Sagiv, *Nature* **318**, 353 (1985).
12. In terms of the resolution-corrected width $W = \{[\mathrm{HWHM}(2\theta)]^2 - [\mathrm{Res}(2\theta)]^2\}^{1/2}$, we have $L = 0.45\lambda/(W\cos\theta)$, where λ is wavelength. See A. Guinier, *X-ray Diffraction* (Freeman, San Francisco,

1968), chap. 5.1, pp. 121–125.
13. C. W. Bunn and E. R. Howells, *Nature* **174**, 549 (1954).
14. E. S. Clark and L. T. Muus, *Z. Kristallogr.* **117**, 119 (1962).
15. Value based on ab initio molecular orbital calculations on perfluoro-*n*-alkane chains by D. A. Dixon, F. A. van Catledge, B. E. Smart, Abstracts of the 9th International Union of Physical and Applied Chemistry Conference on Physical and Organic Chemistry (1988), p. A15.
16. The extended zigzag conformation of PTFE in a more closely packed arrangement may be obtained in a **B**-centered cell with a = 9.50 Å, b = 5.05 Å, γ = 105.5°, molecular area = 23.1 Å^2, but only at a pressure of at least 450 GPa; see H. D. Flack, *J. Polym. Sci. Part A-2* **10**, 1799 (1972).
17. Z. Berkovitch-Yellin, *J. Am. Chem. Soc.* **107**, 8239 (1985).
18. K. Kjaer *et al.*, in preparation.
19. S. W. Barton *et al.*, *J. Chem. Phys.*, in press.
20. We thank J. B. Lando for discussions and F. Hirshfeld for critical reading of the manuscript. Supported by the U.S./Israel Binational Science Foundation, Jerusalem; the fund for basic research of the Israel Academy of Sciences and Humanities; Stiftung Volkswagenwerk; the Petroleum Fund of the American Chemical Society; and the Danish Foundation for Natural Sciences. We gratefully acknowledge beam time at Hasylab, DESY, Hamburg, FRG.

1 June 1988; accepted 7 September 1988

Sugar and Signal-Transducer Binding Sites of the *Escherichia coli* Galactose Chemoreceptor Protein

NAND K. VYAS, MEENAKSHI N. VYAS, FLORANTE A. QUIOCHO

D-Galactose–binding (or chemoreceptor) protein of *Escherichia coli* serves as an initial component for both chemotaxis towards galactose and glucose and high-affinity active transport of the two sugars. Well-refined x-ray structures of the liganded forms of the wild-type and a mutant protein isolated from a strain defective in chemotaxis but fully competent in transport have provided a molecular view of the sugar-binding site and of a site for interacting with the Trg transmembrane signal transducer. The geometry of the sugar-binding site, located in the cleft between the two lobes of the bilobate protein, is novel in that it is designed for tight binding and sequestering of either the α or β anomer of the D-stereoisomer of the 4-epimers galactose and glucose. Binding specificity and affinity are conferred primarily by polar planar side-chain residues that form intricate networks of cooperative and bidentate hydrogen bonds with the sugar substrates, and secondarily by aromatic residues that sandwich the pyranose ring. Each of the pairs of anomeric hydroxyls and epimeric hydroxyls is recognized by a distinct Asp residue. The site for interaction with the transducer is about 18 Å from the sugar-binding site. Mutation of Gly^{74} to Asp at this site, concomitant with considerable changes in the local ordered water structures, contributes to the lack of productive interaction with the transmembrane signal transducer.

BACTERIAL PERIPLASMIC BINDING proteins are essential components of both high-affinity active-transport systems and chemotaxis (*1, 2*). These proteins have three distinct binding sites that can be studied by x-ray crystallography: (i) a fast-reacting and tight-affinity binding site for substrates such as carbohydrates, oxyacid anions, or amino acids (*3*), (ii) a site (or a set of sites) for interacting with other transport protein components lodged in the cytoplasmic membrane, and (iii) a set of sites for interacting with the transmembrane signal transducer protein that is responsible for triggering chemotaxis.

We have determined and crystallographically refined to *R*-factor values of 0.15 to 0.18 the 1.7 Å structures of the L-arabinose–binding (ABP) and sulfate-binding proteins and the 2.4 Å structures of the leucine-isoleucine-valine- and leucine-specific binding proteins (*4–8*). Recently we determined the D-maltose–binding protein structure at 2.8 Å (*9*) and, as we report, the refinement of the D-galactose–binding protein at 1.9 Å. The tertiary structures of the six proteins, representing about a third of the entire family of binding proteins, are similar despite minimal sequence homology; they are ellipsoidal and are composed of two distinct but similar globular domains that are connected by three separate peptide segments (for example, Fig. 1). The single substrate-binding site of each protein is located in an essentially identical cleft between the two domains. Perhaps the most striking common feature of these proteins is that the diverse substrates are bound mainly by hydrogen bonds (*4, 5, 7, 9*). These structural studies have also led to molecular understanding of protein-sugar interactions (*10, 11*) and of electrostatic interactions in protein structures and in binding of charged substrates (*12*).

To locate other functional sites, we stud-

Howard Hughes Medical Institute and Departments of Biochemistry and of Physiology and Molecular Biophysics, Baylor College of Medicine, Houston, TX 77030.

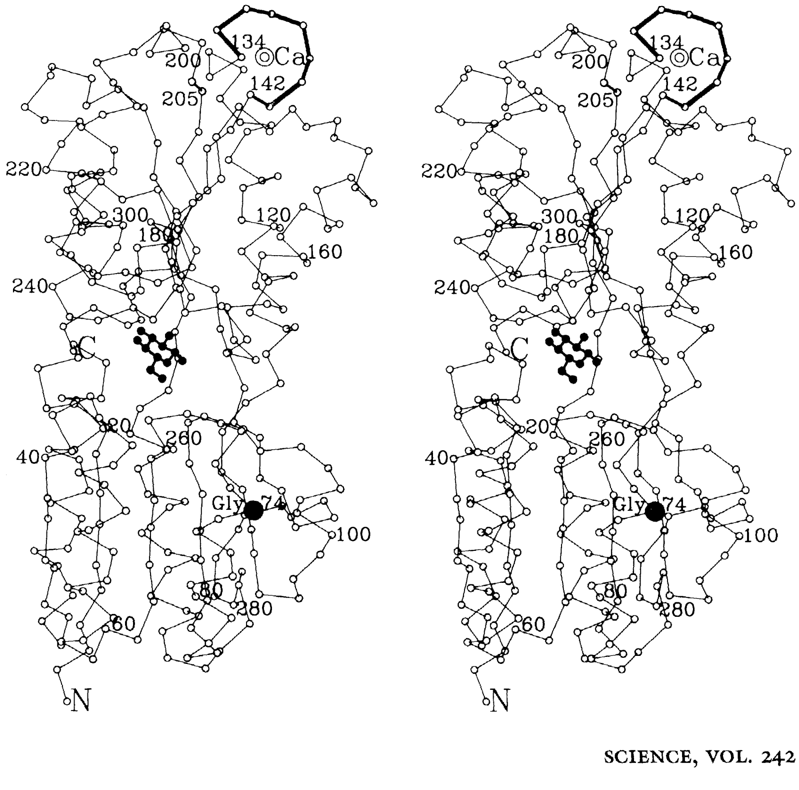

Fig. 1. α-Carbon backbone trace of the GBP structure refined at 1.9 Å resolution. Especially highlighted are: (i) the model of the β-D-glucose substrate (filled circles) buried in the cleft formed between the two domains; (ii) calcium (depicted as a double circle) bound in a loop (thicker lines) composed mainly of residues 134 to 142 located at one end of the elongated molecule [for details see (*6*)]; and (iii) Gly^{74} (large filled circle), which is part of a site for interacting with the Trg transmembrane signal transducer. The orientation of the two domains is such that the amino termini of all the helices and carboxyl termini of all the strands point to the cleft between the two domains.